INTERNATIONAL JOURNAL FOR NUMERICAL METHODS IN BIOMEDICAL ENGINEERING
Int. J. Numer. Meth. Biomed. Engng. 2013; **29**:217–232
Published online 18 October 2012 in Wiley Online Library (wileyonlinelibrary.com). DOI: 10.1002/cnm.2520

A computationally efficient framework for the simulation of cardiac perfusion using a multi-compartment Darcy porous-media flow model

C. Michler[1], A. N. Cookson[1], R. Chabiniok[1], E. Hyde[2], J. Lee[1], M. Sinclair[1], T. Sochi[1], A. Goyal[1], G. Vigueras[1], D. A. Nordsletten[1] and N. P. Smith[1,2,*,†]

[1]*Department of Biomedical Engineering, King's College London, King's Health Partners, St. Thomas' Hospital, London, SE1 7EH, UK*
[2]*Department of Computer Science, University of Oxford, Oxford, OX1 3QD, UK*

SUMMARY

We present a method to efficiently simulate coronary perfusion in subject-specific models of the heart within clinically relevant time frames. Perfusion is modelled as a Darcy porous-media flow, where the permeability tensor is derived from homogenization of an explicit anatomical representation of the vasculature. To account for the disparity in length scales present in the vascular network, in this study, this approach is further refined through the implementation of a multi-compartment medium where each compartment encapsulates the spatial scales in a certain range by using an effective permeability tensor. Neighbouring compartments then communicate through distributed sources and sinks, acting as volume fluxes. Although elegant from a modelling perspective, the full multi-compartment Darcy system is computationally expensive to solve. We therefore enhance computational efficiency of this model by reducing the N-compartment system of Darcy equations to N pressure equations, and N subsequent projection problems to recover the Darcy velocity. The resulting 'reduced' Darcy formulation leads to a dramatic reduction in algebraic-system size and is therefore computationally cheaper to solve than the full multi-compartment Darcy system. A comparison of the reduced and the full formulation in terms of solution time and memory usage clearly highlights the superior performance of the reduced formulation. Moreover, the implementation of flux and, specifically, impermeable boundary conditions on arbitrarily curved boundaries such as epicardium and endocardium is straightforward in contrast to the full Darcy formulation. Finally, to demonstrate the applicability of our methodology to a personalized model and its solvability in clinically relevant time frames, we simulate perfusion in a subject-specific model of the left ventricle. Copyright © 2012 John Wiley & Sons, Ltd.

Received 1 May 2012; Revised 10 August 2012; Accepted 19 September 2012

KEY WORDS: cardiac perfusion; multi-compartment modelling; Darcy flow; porous-media flow; finite-element modelling

1. INTRODUCTION

Coronary perfusion is the mechanism by which the heart is supplied with oxygen and nutrients while waste products are being removed through a network of blood vessels. The numerical simulation of coronary perfusion enables a more quantitative analysis of perfusion data and has the potential to play a vital role in advancing the understanding of important aspects of coronary flow dynamics [1–3] and improve medical diagnosis and treatment [4]. However, the subject-specific simulation of perfusion faces several major challenges. To date, it has been very difficult to obtain accurate anatomical information of the complete human coronary vascular network, ranging from the millimetre to the micrometre scale. In cases where such detailed information has been

*Correspondence to: N. P. Smith, Department of Biomedical Engineering, King's College London, King's Health Partners, St. Thomas' Hospital, London, SE1 7EH, UK.

†E-mail: nicolas.smith@kcl.ac.uk

obtained from experiments, this comes at the price of destroying the heart sample itself and, therefore, is an approach that is clearly unsuitable for patient-specific modelling. Furthermore, even if one had exact anatomical information available, simulating blood flow within clinically relevant time scales on such a vast vascular network represents a significant challenge in terms of computational complexity.

Perfusion models have sought to address these issues by modelling vascular flow as Darcy porous-media flow where the permeability tensor encapsulates the homogenized vasculature [5–7]; for the general theory on porous media flow, see [8]. Moreover, applying this approach to the vasculature within specified ranges of vessel diameter allows us to treat each range of length scales as a compartment characterized by its own permeability tensor. In addition to the computational advantages outlined earlier, such a porous-media flow model also constitutes an attractive surrogate model for cardiovascular blood flow modelling in the clinical context, in the sense that it can be directly validated using perfusion scans imaging the transport of contrast agent within the coronary blood pool. However, current perfusion models are typically oversimplified. Some models neglect vascular connections between non-neighbouring compartments [9], whereas other models allow for uninhibited flow within compartments in contrast to experimental evidence suggesting that the myocardium is partitioned into perfusion regions that are perfused by distinct arterial networks [10]. To overcome these deficiencies, we have previously proposed a multi-compartment Darcy poro-elastic model of cardiac perfusion, which accounts for such regions and connections between non-neighbouring compartments and derives its parameters from vascular cryomicrotome data [11].

Specifically within this model, the vascular network is represented as an hierarchy of fluid compartments, each of which corresponds to a certain range of length scales and is characterized by an effective permeability tensor and porosity. These compartments co-exist on the same spatial domain and communicate through distributed coupling terms acting as sources and sinks. Such intercompartment coupling terms, intracompartment permeability tensors and porosities are derived from the vasculature through averaging or homogenization across specified ranges of length scales effectively encapsulating the vascular anatomical data. The number of compartments N is, in principle, arbitrary and can be adjusted to the detail of available data. This allows, for instance, the investigation of diseases that target primarily large or small vessels, which, accordingly, manifests itself within the compartment of corresponding length scales. Because the vascular data derives from isolated pig hearts, the heart does not undergo any motion, and hence here, we do not account for the effect of large deformation. For studies considering the effect of large deformation on perfusion, we refer to Refs. [6, 11, 12].

In this paper, we enhance the computational efficiency of this approach by reducing the N-compartment system of Darcy equations to N pressure equations of Poisson type, eliminating the Darcy law by substitution. For the standard Darcy system, that is without multiple compartments, such a reduction to a pressure equation, or 'reduced' Darcy formulation as we shall refer to it, has been previously performed in Refs. [13–15]. The resulting reduced Darcy model offers several advantages in comparison with the full formulation. A dramatic reduction in the size of the algebraic system can be obtained, and moreover, the implementation of flux and, more specifically, impermeable boundary conditions on arbitrarily curved boundaries is straightforward. To assess the respective performance of the reduced and the full formulation, we compare each approach in terms of solution time and memory usage for a given discretization error tolerance. Although the full formulation experiences a disproportionate deterioration of solve time and memory usage with the number of Darcy compartments, the reduced formulation mitigates such deterioration and renders the methodology applicable to realistic geometries with many DOFs. We demonstrate the potential of the proposed methodology by showing a clinically motivated application of simulating perfusion in a left ventricle on a subject-specific geometry using physiological flow rates derived from microsphere-count experimental data.

The remainder of the paper is organized as follows: Section 2 presents the governing equations of the Darcy multi-compartment model and derives its reduced form. Section 3 establishes the discretization of the full and reduced Darcy multi-compartment formulations. In Section 4, we present a convergence study for the full and reduced Darcy formulation, and compare the two formulations in terms of solution time, memory usage and accuracy. In Section 5, we progress the proposed

DOI: 10.1002/cnm

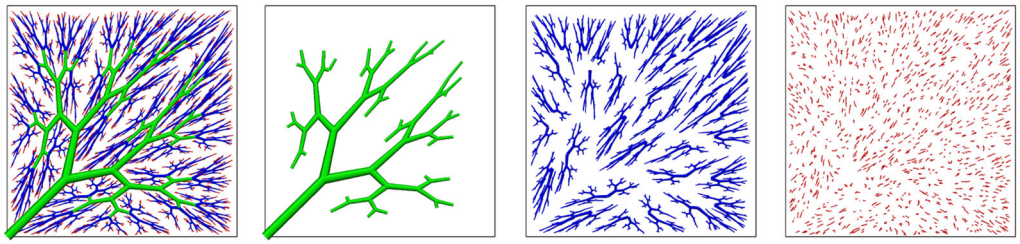

Figure 1. (a) Illustration of a region where vessels of a large range of length scales exist in close proximity. (b)–(d) Illustration of the concept of scale separation into three spatially coexisting compartments. The choice of the number of compartments is, in principle, arbitrary, but is motivated by considerations of available vascular anatomy and computational resources to maximise personalization of the model.

methodology to the perfusion simulation in a subject-specific left ventricle model. Section 6 contains concluding remarks.

2. A MULTI-COMPARTMENT POROUS-MEDIUM DARCY-FLOW MODEL

As outlined previously, we model perfusion in the static myocardium as porous-media flow governed by Darcy's equation. To capture the characteristic vascular features across a range of spatial scales of several orders of magnitude, we compartmentalize the vasculature into spatially co-existing compartments associated with a particular range of length scales. In each compartment, the vascular structure and, specifically the vessel diameter and orientation, is effectively captured by the porosity and intracompartment permeability tensor field for each compartment and by an intercompartment coupling term through which different compartments exchange mass. For the determination of these parameters from real anatomical data, we refer to Ref. [11].

2.1. Governing equations of the full Darcy multi-compartment model

Before introducing the multi-compartment Darcy model, let us recall the *classical* Darcy system

$$\boldsymbol{w} + \boldsymbol{K} \cdot \nabla p = \boldsymbol{0} \quad \text{in } \Omega\,, \tag{1a}$$

$$\nabla \cdot \boldsymbol{w} = s \quad \text{in } \Omega\,, \tag{1b}$$

where $\boldsymbol{w}$ and p denote the Darcy velocity and pore pressure, respectively, $\boldsymbol{K}$ is the permeability tensor (positive definite) of the porous solid and s is a source or sink. Equations (2a) and (2b) are set on an open bounded region $\Omega \subset \mathscr{R}^n$ with space dimension n and piecewise smooth boundary Γ.

A limitation of the classical Darcy system (1) is its inability to accurately capture flow in regions where vessels of a large range of length scales exist in close proximity as is the case in the myocardium, as illustrated in Figure 1. Straight homogenization would result in a flow field that is inaccurate because of the disparity of length scales and associated flow features in close spatial proximity. As a consequence, it would be impossible to accurately compute associated physics of interest such as advective transport, for instance. To overcome this limitation, we adopt a 'compartmentalisation' approach, that is, we apply the same concept of averaging or homogenization now to specified ranges of length scales, resulting in multiple Darcy systems that co-exist on the same spatial domain; see Figure 2 for a schematic illustration.

Extending the classical Darcy system (1) to the *multi-compartment* Darcy system of N compartments, we can write the Darcy system for compartment $i \in [1, N]$ as follows[‡]

$$\boldsymbol{w}_i + \boldsymbol{K}_i \cdot \nabla p_i = \boldsymbol{0} \quad \text{in } \Omega\,, \tag{2a}$$

[‡]no summation over repeated indices unless stated otherwise.

DOI: 10.1002/cnm

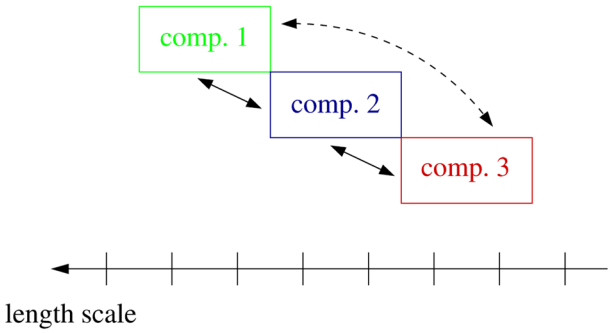

Figure 2. Schematic illustration of the concept of scale separation into spatially coexisting compartments and the possibility of non-hierarchical connections (– – –) in addition to the purely hierarchical ones (—) for the region with vessels of a large range of length scales in close proximity depicted in Figure 1.

$$\nabla \cdot \boldsymbol{w}_i + \sum_{k=1}^{N} \beta_{i,k}(p_i - p_k) = s_i \quad \text{in } \Omega\,, \tag{2b}$$

where subscript i indicates compartment-specific quantities and $\beta_{i,k} \in \mathscr{R}_0^+$ is the intercompartment coupling coefficient with $\beta_{i,k}$ being symmetric, that is, $\beta_{i,k} = \beta_{k,i}$. The summation term in the mass conservation equation (2b) accounts for the mass exchanged between the fluid compartments i and k, while the exchange of momentum is assumed negligible. These mass fluxes between compartments i and k are assumed proportional to the difference in pressure between compartments i and k.

Note that Equations (2a) and (2b), for the multi-compartment Darcy model, are specified on the same domain Ω, that is, all compartments are spatially co-existing, and each compartment simultaneously occupies a fractional volume of Ω according to the porosity associated with each compartment.

We remark that the formulation of the multi-compartment model can be viewed as an extension of the double-porosity network presented in Ref. [8] to an N-porosity network. Moreover, unlike the strictly hierarchical model of [14], where connections exist only between neighbouring compartments, that is

$$\begin{cases} \beta_{i,k} & \in \mathscr{R}^+ \quad i-1 \leqslant k \leqslant i+1; \\ \beta_{i,k} & 0 \qquad \text{else}\,, \end{cases} \tag{3}$$

the model developed here assumes a network structure such that connections may exist between a compartment and every other compartment, that is,

$$\beta_{i,k} \in \mathscr{R}_0^+ \quad i,k = 1,\ldots,N\,, \tag{4}$$

which is schematically illustrated in Figure 2. In that respect, the strictly hierarchical model of [14] is a special case of the more general model considered here.

A conservative mass exchange implies that the mass drained from (fed into) compartment i equals the mass fed into (drained from) compartment k, which requires $\beta_{i,k}$ to be symmetric, as stated earlier under Equations (2a) and (2b). Moreover, the mass of compartment i that is exchanged with itself is obviously zero, thus $\beta_{i,i} = 0$. The symmetry of $\beta_{i,k}$ warrants mass conservation across the hierarchy of compartments

$$\sum_{i=1}^{N}\sum_{k=1}^{N} \beta_{i,k}(p_i - p_k) = 0 \quad \text{in } \Omega\,, \tag{5}$$

DOI: 10.1002/cnm

which implies global mass conservation

$$\sum_{i=1}^{N} \nabla \cdot \boldsymbol{w}_i = \sum_{i=1}^{N} s_i \quad \text{in } \Omega\,. \tag{6}$$

The system (2) is augmented by the following Dirichlet and Neumann boundary conditions, respectively,

$$\boldsymbol{w}_i \cdot \boldsymbol{n} = \psi_i \quad \text{on } \Gamma_{\mathrm{D}}\,, \tag{7a}$$

$$p_i \boldsymbol{n} = g_i \boldsymbol{n} \quad \text{on } \Gamma_{\mathrm{N}}\,, \tag{7b}$$

where $\boldsymbol{n}$ denotes the unit outward normal vector, ψ_i is the normal component of the velocity field on the boundary and $\boldsymbol{g}_i$ are given boundary tractions. We further assume that $\Gamma_{\mathrm{D}} \cup \Gamma_{\mathrm{N}} = \Gamma$ with $\Gamma_{\mathrm{D}}, \Gamma_{\mathrm{N}} \notin \emptyset$.

2.2. Governing equations of the reduced Darcy multi-compartment model

Upon substituting Equation (2a) into (2b), we can eliminate velocity and obtain an equation that is solely written in terms of pressure, and that we refer to as the 'reduced' Darcy formulation, which for compartment i yields

$$-\nabla \cdot (\boldsymbol{K}_i \cdot \nabla p_i) + \sum_{k=1}^{N} \beta_{i,k}(p_i - p_k) = s_i \quad \text{in } \Omega\,, \tag{8}$$

augmented with the following Dirichlet and Neumann boundary conditions,

$$p_i = g_i \quad \text{on } \Gamma_{\mathrm{N}}\,, \tag{9a}$$

$$(-\boldsymbol{K}_i \cdot \nabla p_i) \cdot \boldsymbol{n} = \psi_i \quad \text{on } \Gamma_{\mathrm{D}}\,, \tag{9b}$$

where g_i are given boundary pressures, $\boldsymbol{n}$ denotes the unit outward normal vector and ψ_i is essentially the normal component of the Darcy velocity at the boundary. Note that in contrast to the full Darcy formulation, in the reduced model, the specification of pressure constitutes a Dirichlet boundary condition. However, it is applied on the portion of Γ that in Section 2.1 has been denoted as Γ_{N}; and vice versa for the normal component of the Darcy velocity.

Upon obtaining the pressure solution of (8), the corresponding Darcy velocity can be derived from

$$\boldsymbol{w}_i = -\boldsymbol{K}_i \cdot \nabla p_i \quad \text{in } \Omega\,. \tag{10}$$

3. VARIATIONAL FORMULATION AND DISCRETIZATION OF THE GOVERNING EQUATIONS

Although on the continuous level and for sufficiently smooth solutions, the solution of the system (2) is obviously equivalent to the solution of the pressure equation (8) with subsequent projection (10), under discretization, this only holds up to a certain bound. In this section, we first present the discretization of the full Darcy system, followed by that of the reduced formulation.

3.1. Discretization of the full Darcy multi-compartment model

The variational formulation of the multi-compartment Darcy system (2) can be expressed for compartment i as follows: Given the components of $\boldsymbol{K}_i$, $\beta_{i,k}$ and $s_i \in L^{\infty}(\Omega)$, find $\boldsymbol{w}_i \in \mathscr{V}_i$, $p_i \in \mathscr{Q}_i$ such that for all $\boldsymbol{v}_i \in \mathscr{V}_i$, $q_i \in \mathscr{Q}_i$

$$\left(\boldsymbol{v}_i, \boldsymbol{K}_i^{-1}\boldsymbol{w}_i\right)_{\Omega} - (\nabla \cdot \boldsymbol{v}_i, p_i)_{\Omega} + (\boldsymbol{v}_i, g_i \boldsymbol{n})_{\Gamma_{\mathrm{N}}} + (q_i, \nabla \cdot \boldsymbol{w}_i)_{\Omega} + \left(q_i, \sum_{k=1}^{N} \beta_{i,k}(p_i - p_k)\right)_{\Omega} = (q_i, s_i)_{\Omega}\,, \tag{11a}$$

DOI: 10.1002/cnm

where $(\cdot,\cdot)$ denotes the $L^2(\Omega)$ inner product,

$$\mathscr{V}_i = \boldsymbol{H}_{\mathrm{D}}(\mathrm{div},\Omega) = \left\{\boldsymbol{v}|\boldsymbol{v}\in\left(L^2(\Omega)\right)^{n_d},\quad \mathrm{div}\boldsymbol{v}\in\left(L^2(\Omega)\right),\quad \mathrm{trace}(\boldsymbol{v}\cdot\boldsymbol{n}) = \psi_i \in H^{1/2}(\Gamma_{\mathrm{D}})\right\},$$
$$\mathscr{Q}_i = L^2(\Omega) = \left\{p|p\in L^2(\Omega)\right\}. \tag{11b}$$

Discretization of the variational problem (11) is obtained by replacing the infinite-dimensional function spaces by finite-dimensional subspaces. For the discrete setting, we use nodal Lagrange elements with basis functions that are in $H^1(\Omega)$ rather than $\boldsymbol{H}(\mathrm{div},\Omega)$ with the assumption that the given data for the problem results in a solution that is in $H^1(\Omega)$.

To obtain a stable and convergent numerical discretization of the classic Darcy system, that is, for a single compartment and without coupling terms, the discrete velocity and pressure spaces must satisfy the Babuška–Brezzi condition, also referred to as inf-sup condition, which is a condition on the compatibility of the interpolation spaces used for velocity and pressure; see Refs. [16, 17]. To this end, mixed formulations are typically employed, that is, different interpolations are used for velocity and pressure where the latter must not be of too high in order, otherwise the inf-sup condition is violated. In this paper, we therefore generally use a pressure approximation that is one order lower than the one for velocity for the full Darcy formulation. Alternatively, stabilization techniques can be employed to circumvent the inf-sup condition and ensuing restrictions on the choice of interpolation spaces [18, 19].

3.2. Discretization of the reduced Darcy multi-compartment model

The ensuing variational statement of (8) is as follows: Find $p_i \in \mathscr{Q}_i$ such that for all $q_i \in \mathscr{Q}_i$

$$(\nabla q_i, \boldsymbol{K}_i\cdot\nabla p_i)_\Omega + (q_i,\psi_i)_{\Gamma_{\mathrm{D}}} + \left(q_i, \sum_{k=1}^{N}\beta_{i,k}(p_i-p_k)\right)_\Omega = (q_i,s_i)_\Omega\,, \tag{12}$$

where

$$\mathscr{Q}_i = H^1(\Omega) \tag{13}$$

and satisfies the boundary conditions specified in Equations (9a) and (9b).

We emphasize that for the reduced Darcy formulation imposing flux and, more specifically, impermeable boundary conditions on arbitrarily curved surfaces is straightforward by virtue of the boundary flux term that appears in Equation (12). In contrast, the full Darcy model requires imposing a condition on the normal velocity component on the boundary (Equation (7a)) which, for cases with arbitrarily curved boundaries, is non-trivial. However, this advantage comes with the caveat that, as the boundary condition must be imposed as a Neumann condition in the reduced formulation, it is enforced in a weak sense as part of the variational statement rather than strongly as a Dirichlet condition as in the full Darcy model.

Subsequently, to obtain the velocity, the discrete form of (10) is evaluated. However, the gradient of the C^0-continuous pressure is only a piecewise continuous function. To obtain a smooth representation of the velocity field, we project the pressure gradient onto a C^0-continuous approximation of the velocity. Find $\boldsymbol{w}_i \in \mathscr{V}_i$ such that for all $\boldsymbol{v}_i \in \mathscr{V}_i$,

$$(\boldsymbol{v}_i,\boldsymbol{w}_i)_\Omega = (\boldsymbol{v}_i, -\boldsymbol{K}_i\cdot\nabla p_i)_\Omega\,. \tag{14}$$

4. NUMERICAL EXPERIMENTS

In Section 4.1, we present convergence results for the full and reduced Darcy formulation, and in Section 4.2, we compare the full and reduced Darcy model in terms of solution time, memory requirements and accuracy.

DOI: 10.1002/cnm

4.1. Convergence tests

To assess convergence of the full and reduced Darcy formulations, we consider a two-dimensional bi-unit square domain with boundary conditions consistent with an analytic solution for pressure of the following form:

$$p = \sin(2\pi x) \cdot \sin(2\pi y)\,, \tag{15}$$

and corresponding velocity field and source term computed using Darcy's law; see also Ref. [18]. For the full Darcy formulation, we apply the normal velocity component as Dirichlet boundary condition (7a), and the source field is included in the conservation equation (2b). For the reduced Darcy formulation, we apply the Neumann boundary condition (9b) consistent with the normal velocity component according to (10), and the source field included in pressure equation (8). In both cases, a corner node was prescribed to the analytic pressure value to set a reference level for the pressure field. For the full Darcy formulation, we use a quadratic approximation of the velocity field and a linear approximation of pressure ($P2/P1$), whereas for the reduced Darcy model, we use a quadratic approximation of both velocity and pressure ($P2/P2$) with nodal Lagrange basis functions. We then compute this problem on a sequence of refined meshes with the following number of elements: 5×5, 10×10, 20×20, 40×40 and 80×80.

Figure 3 plots the error versus the inverse of the mesh size for the $L2$ norm of the errors in velocity and pressure, and for the $H1$ seminorm of the error in pressure. The slope of the different curves allows us to infer the rate of decrease in the discretization error and compare it with the expected values. For the full Darcy model, we observe a rate of decrease in the error in pressure of about 2 in the $L2$ norm and of about 1 in the $H1$ seminorm, which is in agreement with the linear approximation of pressure. The rate of decrease in the error in velocity of about 2 for a quadratic approximation is still in agreement with theoretical predictions due to a bound on the rate of decrease in the error in pressure. For the reduced Darcy formulation, we observe a rate of decrease in the error in pressure of about 3 and 2 for the $L2$ norm and $H1$ seminorm, respectively, which conforms to a quadratic approximation of pressure. Moreover, the rate of decrease in the error in velocity of about 2 for a quadratic approximation emanates from the projection of the pressure gradient and is consistent with the rate of 2 for the $H1$ seminorm of the pressure error. All the rates of decrease in discretization error observed in Figure 3 are therefore in agreement with theoretical predictions.

4.2. Comparison of full versus reduced-Darcy formulation

To assess the computational efficiency of the full and the reduced Darcy formulations for a varying number of compartments, in this section, we carry out numerical experiments on a simple cube

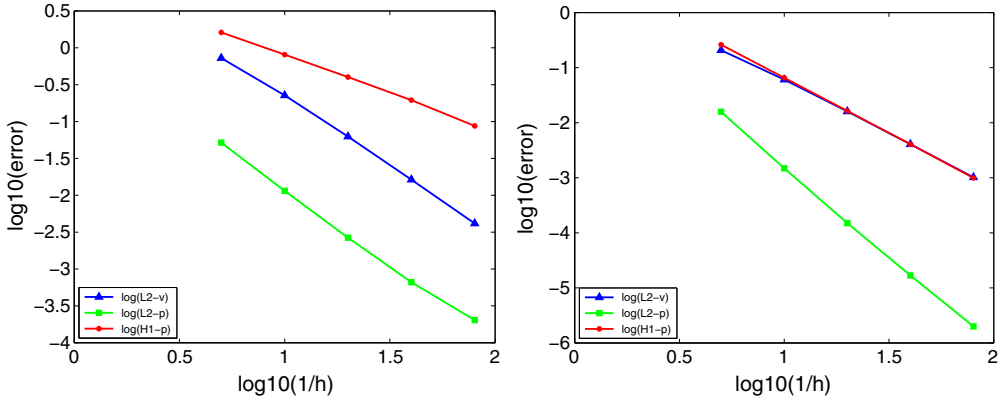

Figure 3. Convergence of the full Darcy formulation using a ($P2/P1$) approximation of velocity/pressure (left) and of the reduced Darcy formulation using a (P2/P2) approximation (right): Error versus inverse of element size in double log scale. The average slope for $\log(L2-v)$, $\log(L2-p)$ and $\log(H1-p)$ for the full Darcy formulation are -1.9, -2.0 and -1.1, respectively, and for the reduced Darcy formulation, they are -1.9, -3.2 and -2.0, respectively.

DOI: 10.1002/cnm

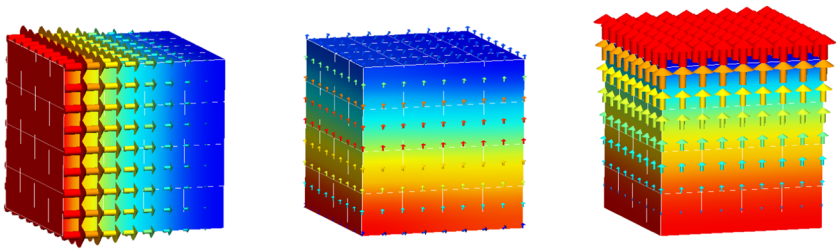

Figure 4. Illustration of the problem setup of the cube problem to assess the accuracy of the full and reduced Darcy formulations versus the solution time for a varying number of compartments and discretization parameters. Here, a three-compartment model with compartmental pressures plotted on the surfaces and velocity vectors, scaled and coloured by their magnitude (amplification factor of 100 used for velocities in compartment 2 for ease of visualization) for compartments 1–3 (left to right). Boundary conditions are as follows: Inflow BC according to Equation (9b) on the left face of compartment 1, all boundaries impermeable in compartment 2, outflow BC according to Equation (9b) on the top face of compartment 3, all other boundaries impermeable.

problem with a specified inflow boundary condition in compartment 1 on the left face and an outflow boundary condition on the final compartment on the top face; all other faces are set impermeable. For an illustration of the problem setup, see Figure 4. In this scenario, the flow enters compartment 1, then conducts through subsequent compartments until it leaves the domain in the final compartment through the outflow face with the permeability in all compartments being isotropic. As in Section 4.1, we use a $(P2/P1)$ approximation for the full Darcy formulation and a $(P2/P2)$ approximation for the reduced Darcy formulation.

To compare the full and reduced Darcy formulation in terms of solution time and memory usage, we use a direct solver only (i.e. MUMPS [20]), because for an iterative solver, the performance hinges on the preconditioner invoked and its suitability for the underlying algebraic system. Hence, a given preconditioner may be better suited for certain matrices from one of the models and, thus, bias the results. Moreover, to minimize a possible effect of external processes, the solution time has been averaged over multiple runs. The computations were carried out on a workstation with 2.7 GHz Intel Xeon CPUs and 48 GB of RAM (Intel Corp., Sta. Clara, CA, USA).

Figures 5 and 6 show matrix solution time[§] and memory usage for the full and the reduced Darcy formulations for 1 to 5 compartments, and Figure 5 (right) specifically shows the increase in solution time as a function of the number of porous-flow compartments. For ease of comparison, in Figures 5 (left) and 6, we have chosen to plot the solution time and memory usage, respectively, against the rank of the combined pressure and velocity system also for the reduced formulation in this context. Figure 5 (left) conveys that the number of pressure and velocity DOFs that can actually be solved for the reduced formulation for the same computational cost is larger than for the full formulation resulting in a more accurate solution. Figure 5 (right) shows that, for a given number of flow compartments, the reduced Darcy formulation is about one order of magnitude faster to solve than the full formulation. Moreover, Figure 6 demonstrates that the reduced formulation is cheaper in terms of memory usage than the full formulation.

To analyse the solution time and memory usage characteristics of the two formulations, we plot in Figure 7 (left) and (right) the structure of the system matrix for the full and the reduced Darcy formulation, respectively, for a three-compartment case. For the full formulation, pressure and velocity block, diagonal matrices have been marked in Figure 7 (left). For the reduced formulation, Equation (8) corresponding to the pressure equation and the projection step given by Equation (10) can be solved sequentially. In fact, the solution of the latter only requires to build the mass matrix for projection once and then solve the system for multiple right-hand sides corresponding to the

[§]The matrix solution time accounts for most of the total run time, especially as the matrix system gets bigger. We choose here to compare in terms of matrix solution time to assess the implications of the multi-compartment coupling on the resulting matrix structure and the time spent on solving the matrix system.

DOI: 10.1002/cnm

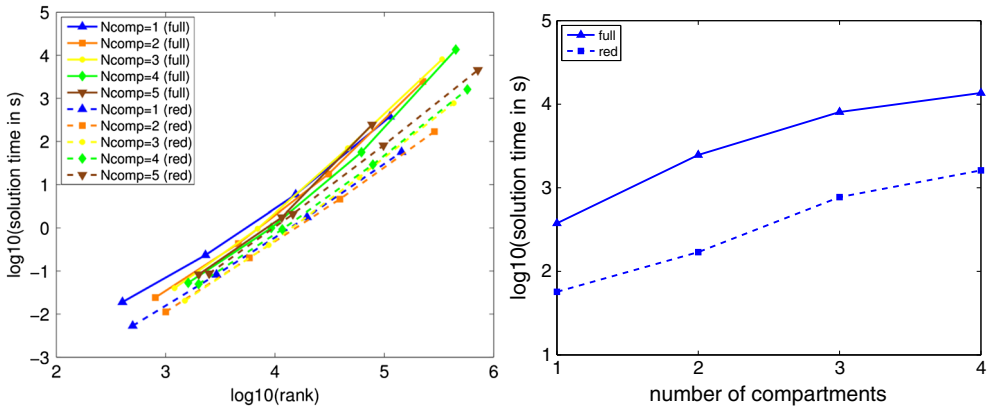

Figure 5. Matrix solution time plotted versus the rank for full and reduced Darcy formulations for a varying number of compartments (1–5) (left). Matrix solution time plotted versus the number of compartments for the full and reduced Darcy formulations for an $8 \times 8 \times 8$ element mesh (right).

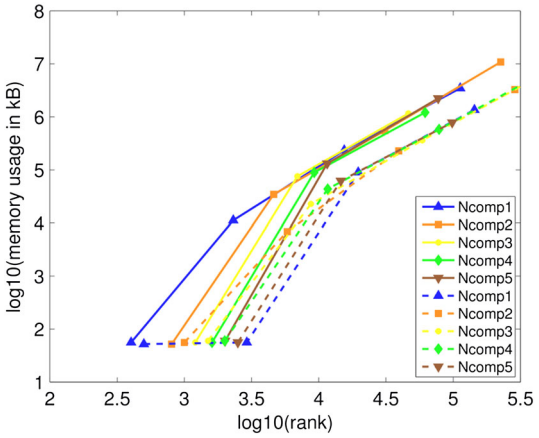

Figure 6. Memory usage plotted versus the rank for the full Darcy formulation (—) and the reduced-Darcy model (– – –) for a varying number of compartments (1–5).

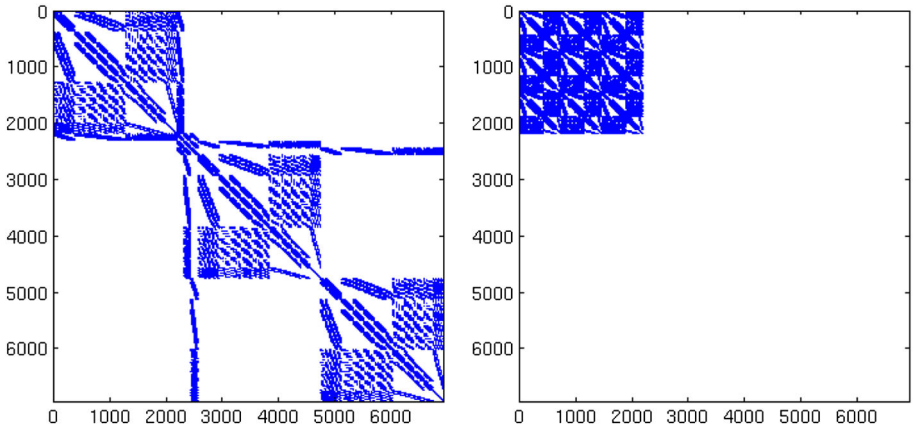

Figure 7. Structure of the system matrix for the full Darcy formulation (left) and for the reduced Darcy formulation with pressure block matrix only (right) for a three-compartment case and a $4 \times 4 \times 4$ element mesh with quadratic velocity and linear pressure approximation (full Darcy) and a quadratic pressure (and quadratic velocity) approximation (reduced Darcy), for exemplification. Rank, condition number and number of non-zeros of the full Darcy system are, respectively, 6, 936, $7.48 \cdot 10^8$ and $4.36 \cdot 10^5$; for the reduced Darcy system (pressure equation; Figure 7 (right)) they are, respectively, 2, 187, $4.97 \cdot 10^7$ and $3.23 \cdot 10^5$.

DOI: 10.1002/cnm

pressure in the different compartments, which is comparatively inexpensive. We therefore plot in Figure 7 (right) only the block matrix resulting from the pressure equation (8). Such decoupling is not possible for the matrix of the full Darcy formulation where a set of N Darcy systems (2) needs to be solved as a single coupled system.

Some key matrix statistics, that is, rank and condition number, are plotted in Figure 8, indicating a reduction in rank and condition number for the reduced formulation when compared with the full formulation, which is also reflected in the lower memory footprint and solution time plotted in Figures 5 and 6.

From these results, it appears that it is simply the rank of the algebraic system of N coupled Darcy systems that induces a deterioration of memory usage and solution time for the full Darcy formulation. In contrast, for the reduced Darcy formulation, such deterioration in memory usage and solution time is mitigated as a result of the decoupling of the pressure equation (12) from the equation for obtaining velocity, Equation (14).

Next, in Figure 9, we assess the accuracy of the pressure and velocity solution obtained with the full and the reduced Darcy formulations for different meshes ($2 \times 2 \times 2$, $4 \times 4 \times 4$ and $8 \times 8 \times 8$ elements), using the solution on the mesh with $16 \times 16 \times 16$ elements as a reference solution. The figure shows that the solution obtained with the reduced Darcy formulation is more accurate than

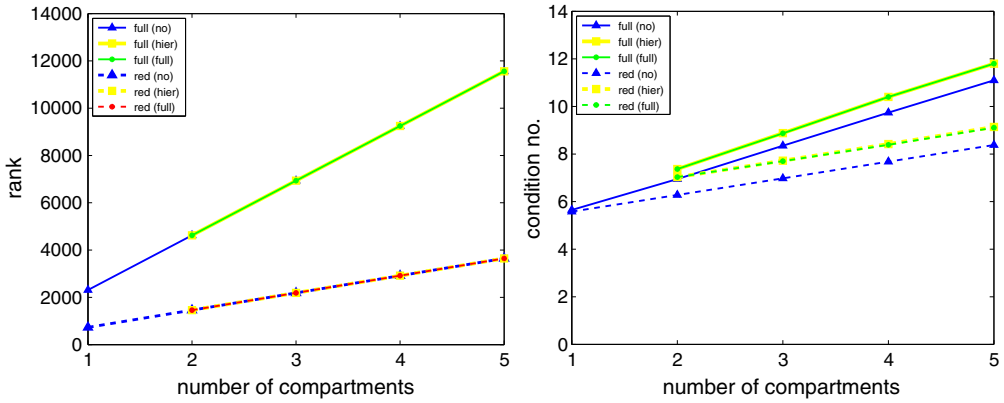

Figure 8. Rank (left) and condition number (right) versus the number of compartments for the full Darcy formulation (—) and the reduced-Darcy model (– – –). Results are shown for no coupling ('no'), hierarchical coupling ('hier', coupling between neighbouring compartments only) and full coupling ('full', coupling between any two compartments).

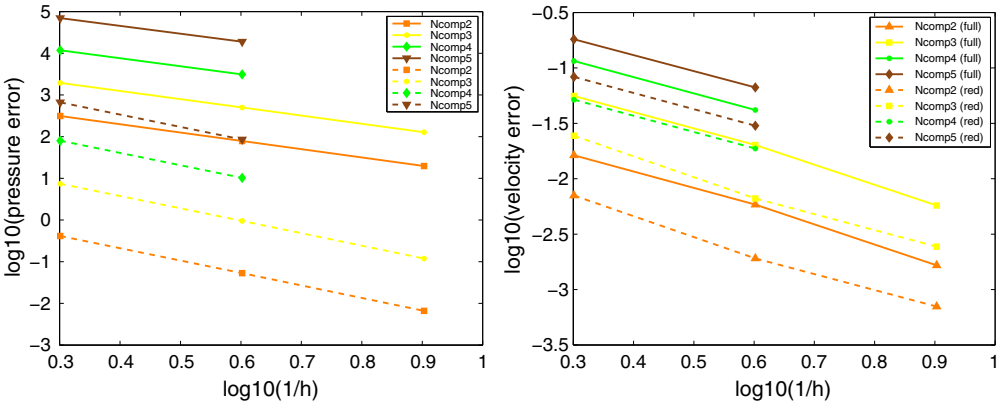

Figure 9. Error in the pressure solution (left) and velocity solution (right) versus the inverse of element size for multi-compartment full Darcy model (—) and reduced-Darcy model (– – –) for varying number of compartments $N = 1, \ldots, 5$.

DOI: 10.1002/cnm

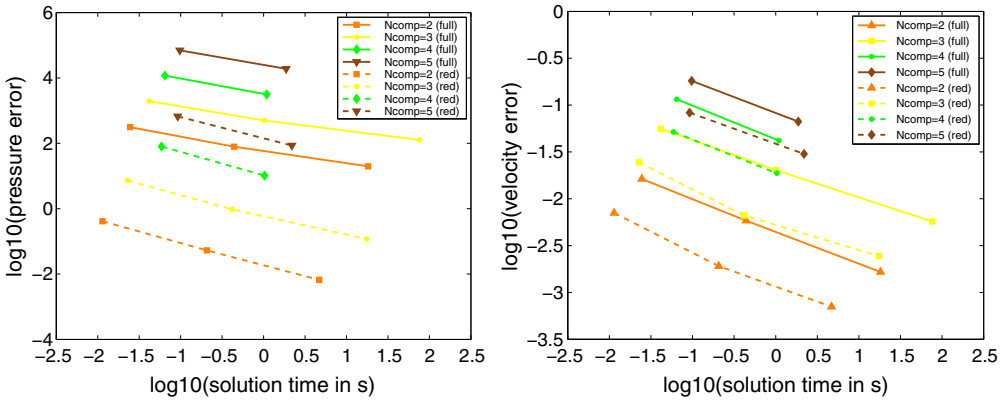

Figure 10. Error in the pressure solution (left) and velocity solution (right) versus solution time for multi-compartment full Darcy model (—) and reduced-Darcy model (– – –) for varying number of compartments $N = 1, \ldots, 5$.

the one obtained with the full formulation for both pressure and velocity. Figure 10 plots the error in the pressure and velocity solution versus the solution time, which can be regarded as a measure of computational efficiency. This plot demonstrates that the reduced Darcy formulation is far more efficient than the full formulation in that, for a given number of compartments, it attains a given error tolerance for a lower computational cost.

5. SUBJECT-SPECIFIC PERFUSION SIMULATION ON LEFT-VENTRICULAR GEOMETRY

Having established the superior computational performance of the multi-compartment reduced Darcy formulation in Section 4, here, we progress it to an application of clinical relevance and demonstrate its solvability in clinically relevant time frames.

We utilize the multi-compartment reduced Darcy formulation to simulate perfusion on a subject-specific left ventricle (LV) of a pig heart. Fluid inflow is imposed in compartment 1 via source terms s_1 corresponding to a vascular tree with 1735 junctions with an average diameter of 0.4142 mm. We note that although the value of this diameter threshold and, therefore, the number of resulting source locations and their strength is in principle arbitrary, the choice is motivated by the intention to ensure a spatially well-distributed inflow. Moreover, because in the clinical context only the larger epicardial vessels are available from angiography, a larger diameter threshold is closer to what would be taken for a human heart in the clinic. The assessment of the corresponding inflow rates was based on microsphere counts, which is commonly considered the gold standard to determine vascular fractional flow rates. Such microsphere counts have been obtained from pig experiments, where perfusion was quantified by injecting fluorescent microspheres with a diameter of 15 μm into the coronary arteries [21]. To visualize the vascular tree of the left coronary artery, an intravascular dye has been injected and, after hardening, the heart has been frozen and cut into slices of 64 μm, and these slices have then been imaged ('cryomicrotome imaging') [10].

With this cryomicrotome data, a computational mesh of the LV has been generated [22] through manual segmentation of the cryomicrotome images, and the vascular tree of the left coronary artery has been reconstructed (Figure 11). For more details on the procedure as well as an analysis of the vasculature, see Ref. [23].

We simulate perfusion of the LV modelled by a three-compartment Darcy model and with volume sources placed according to the terminal junctions of the vascular tree depicted in Figure 11, and with flow rates given by the microspheres counts. These sources provide compartment 1 of the LV with a total inflow rate of 1200 mm^3/s. Because no vascular model has been obtained for the right coronary artery, the inflow from the right coronary artery into the LV via localized sources was not

DOI: 10.1002/cnm

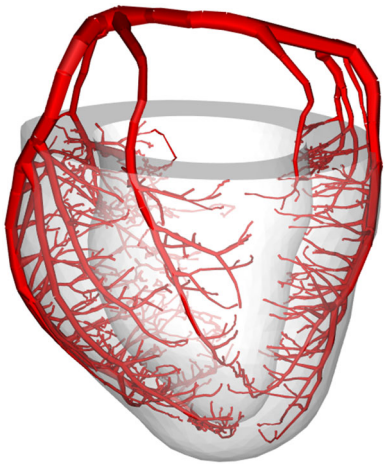

Figure 11. Vascular tree superimposed on the computational geometry of the left ventricle (represented by 24 793 quadratic tetrahedral elements). Sources are placed in compartment 1 at the 1735 terminal junctions of the vasculature with flow rates determined on the basis of microsphere counts from experimental data.

taken into account. Outflow occurs in compartment 3 via a uniform pressure-dependent sink term of the following form:

$$s_3 = -\frac{0.1}{\text{kPa} \cdot \text{s}}(p_3 - 3\ \text{kPa})\,. \tag{16}$$

The material parameters for the Darcy model are taken as follows: Permeability in compartments 1 and 2 is predominant in transmural direction with principal eigenvalues of 1 $\text{mm}^2/(\text{kPa s})$ and 10 $\text{mm}^2/(\text{kPa s})$, respectively, whereas compartment 3 corresponding to the microvascular compartment is assumed isotropic with magnitude of 20 $\text{mm}^2/(\text{kPa s})$. These settings are consistent with the assumption that within a perfusion region, the permeability field obtained from homogenization of the anatomic data of the vasculature is generally reasonably smooth[¶]. The inter-compartment coupling coefficients are taken uniformly as $\beta_{1,2} = 0.02\ (\text{kPa s})^{-1}$ and $\beta_{2,3} = 0.05\ (\text{kPa s})^{-1}$. The LV is represented by a mesh of 24 793 quadratic tetrahedral elements.

Our simulations are subject-specific in that the vasculature, the LV geometry as well as the microsphere-based flow rates for each of the terminal junctions have been obtained directly from experiments, whereas the permeability field has been based on physiologically motivated assumptions, that is, permeability in the microvascular compartment 3 is assumed isotropic and permeabilities in compartments 1 and 2 are assumed predominant in transmural direction. Basing the permeability fields on such assumptions is justified by the fact that, in clinical practice, cryomicrotome data of a patient's vascular tree is not available for parameterization, because it inherently involves the destruction of the heart sample. Therefore, one needs to resort to some assumptions on the variation of permeability as in the current study.

Figure 12 shows the solution for pressure in the three compartments, whereas Figure 13 shows pressure and Darcy velocity magnitude for a cross section through the LV. Pressure and Darcy velocity magnitude are high around the source locations and decrease over subsequent compartments. The pressure values are uniform in the last compartment, as expected in physiological myocardial perfusion. Although the purpose of multi-compartment modelling is precisely to separate the length scales into individual flow compartments, to obtain compartment-specific information about Darcy pressure and velocity, we have also plotted the weighted average of the Darcy pressure

[¶]Although heterogeneous permeabilities might be encountered at perfusion-region boundaries, such heterogeneity can be dealt with by ensuring sufficient mesh resolution in the vicinity of those boundaries.

DOI: 10.1002/cnm

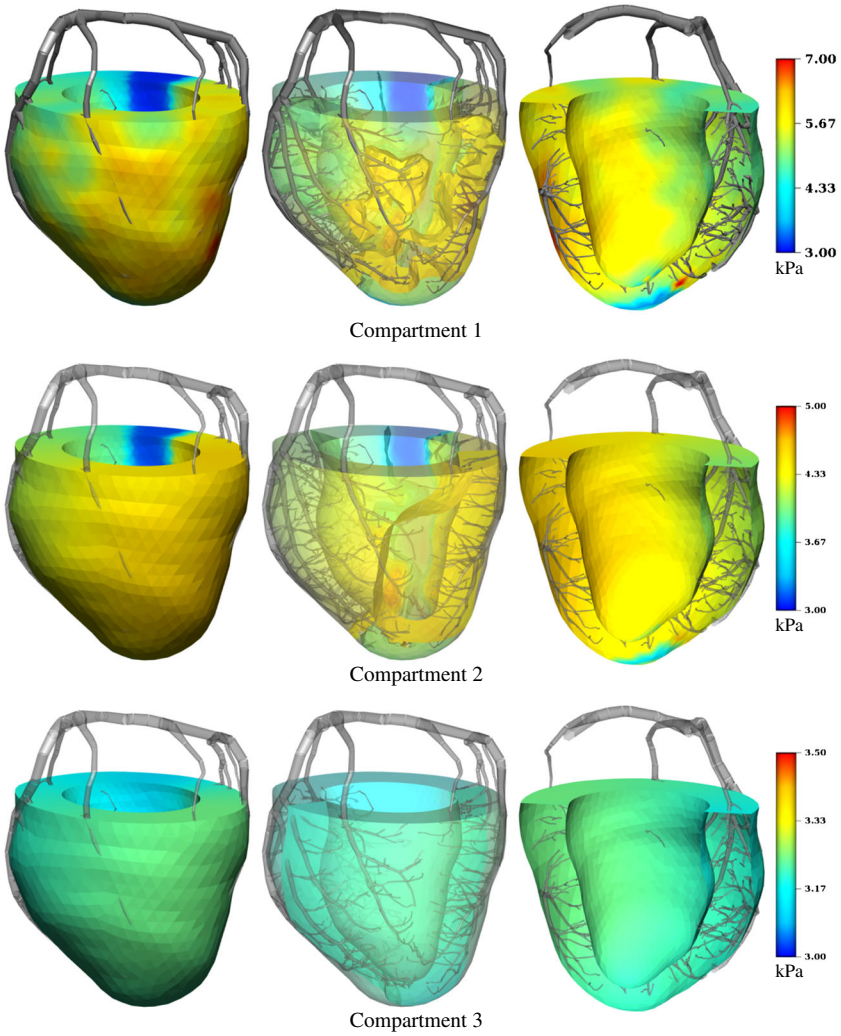

Figure 12. Pressure in compartments 1–3 visualized on the surface (left) and with iso-surfaces of pressure in the volume (center), both with view on the anterior wall, and in a cross section with view on the anterior wall from inside the ventricle with volume removed and internal vessels kept (right) (vasculature shown to indicate location of sources).

in Figure 14, assuming compartment-specific porosities of 0.021, 0.029 and 0.061 for compartments 1–3, respectively, to provide a global view on perfusion. The porosity of compartment 3 corresponding to the microvascular compartment is in line with Ref. [24], and the porosities of compartments 1 and 2 are estimated on the basis of the available anatomic data. In particular, those latter two porosities are derived from the fluid fractional volume of all vessels between 414.2 μm (diameter threshold for the transition from discrete vasculature to homogenized Darcy model) and 64 μm (resolution of the cryomicrotome image data), plus a correction accounting for those vessels that are below the resolution of the cryomicrotome images but not yet accounted for in compartment 3.

The perfusion simulation has been performed using the reduced Darcy formulation, which allows for a straightforward enforcement of impermeable boundary conditions over the base, endocardium and epicardium by simply setting the flux on those boundaries to zero; see Section 3.2 for details. Moreover, the computational efficiency of the reduced formulation enables us to carry out this simulation in about 4 min and requires approximately 2 GB of memory using the direct solver MUMPS [20], whereas the full Darcy formulation takes more than 70 min and requires approximately 17 GB of memory on a workstation with 2.7 GHz Intel Xeon CPUs and 48 GB of RAM.

DOI: 10.1002/cnm

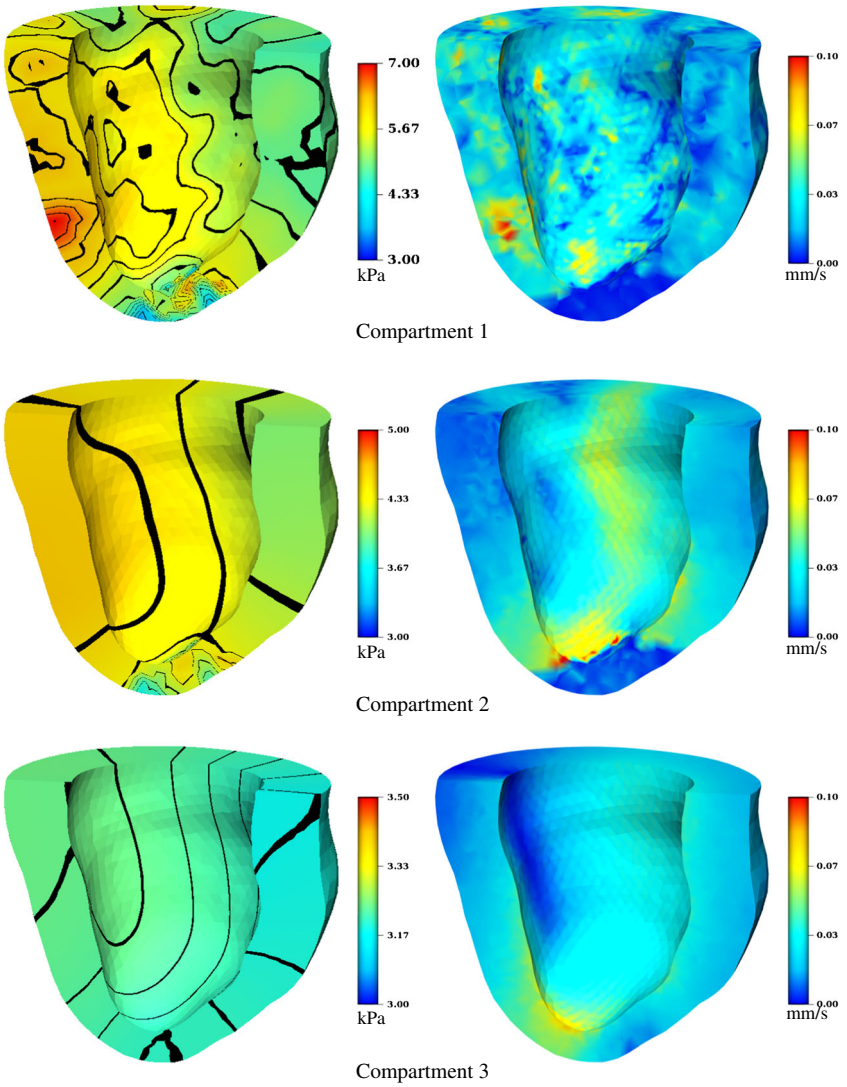

Figure 13. Pressure with isocontours (left) and Darcy velocity magnitude (right) in compartments 1–3. Cross section with view on the anterior wall from inside the ventricle (as in Figure 12 (right)).

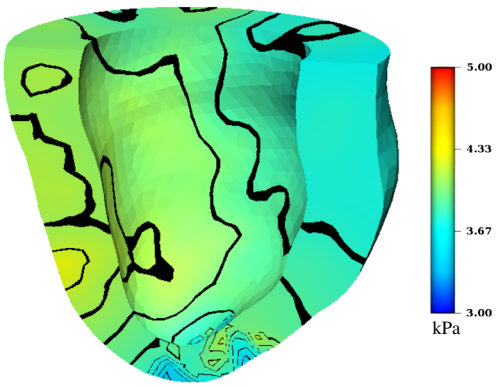

Figure 14. Average pressure with isocontours. Cross section with view on the anterior wall from inside the ventricle (as in Figure 12 (right)).

DOI: 10.1002/cnm

Therefore, for perfusion simulations within clinically relevant time frames, the reduced Darcy formulation provides the opportunity to apply perfusion models in a significantly enlarged set of clinical applications including assessing multiple interventional strategies (e.g. stent position) and/or optimizing diagnostic information acquisition (e.g. contrast agent choice).

6. CONCLUSIONS

We have proposed a method to efficiently simulate cardiac perfusion by means of a multi-compartment porous-media flow model. Multi-compartment modelling enables us to capture length scales in a certain range or 'compartment' by an effective permeability tensor and intercompartment coupling terms. To enhance the computational efficiency, we have reduced the N-compartment system of Darcy equations to N pressure equations, which we also refer to as 'reduced' Darcy formulation. A benefit of the reduced Darcy formulation is that it is straightforward to impose flux, and, specifically, impermeable boundary conditions on curved boundaries such as epicardium and endocardium. However, most notably, the reduced formulation leads to a dramatic reduction in the size of the algebraic system and ensuing cost of memory usage and solution time. Our numerical experiments convey that for a given error tolerance, the reduced Darcy formulation is substantially less expensive in terms of solution time and memory usage than the full formulation. In fact, it is only by virtue of the reduced formulation that cardiac perfusion simulations become feasible in clinically relevant time frames, as demonstrated for a perfusion simulation on a subject-specific left ventricle of a pig heart with physiological inflow rates based on microsphere counts. A comparison of reduced and full formulation on this clinically relevant problem made it clear that the reduced Darcy model is a viable option for carrying out perfusion simulations within time windows that are acceptable to clinical practice.

The presented tools thus constitute a first step towards the translation to the clinic in the context of patient-specific modelling, in particular regarding feasibility in terms of solution time and personalized geometry. However, translation to the clinic furthermore requires the personalization of the material parameters such as permeability and porosity. Moreover, it also requires to account for the effect of large deformations of the tissue on perfusion, which, in the present case of an isolated pig heart, does not apply. These aspects are subjects of ongoing work. Once successfully validated, we intend to use this model to investigate perfusion in the myocardium on a patient-specific basis.

ACKNOWLEDGEMENTS

The authors would like to thank their collaborators at the Academic Medical Center, University of Amsterdam, Department of Medical Physics, Amsterdam, the Netherlands for supplying the cryomicrotome data and Dr. Pablo Lamata, Department of Computer Science, University of Oxford, Oxford, UK for his help in mesh generation.

The authors would also like to acknowledge funding from the EPSRC (EP/G007527/2), the Centre of Excellence in Medical Engineering funded by the Wellcome Trust, the EPSRC under grant number WT 088641/Z/09/Z and the European Commission funded euHeart project (FP7-ICT-2007-224495:euHeart).

REFERENCES

1. Smith NP, Kassab GS. Analysis of coronary blood flow interaction with myocardial mechanics based on anatomical models. *Philosophical Transactions: Mathematical, Physical and Engineering Sciences* 2001; **359**(1783): 1251–1262.
2. Smith NP. A computational study of the interaction between coronary blood flow and myocardial mechanics. *Physiological Measurement* 2004; **25**(4):863.
3. Westerhof N, Boer C, Lamberts RR, Sipkema P. Cross-talk between cardiac muscle and coronary vasculature. *Physiological Reviews* 2006; **86**(4):1263–1308.
4. Smith N, de Vecchi A, McCormick M, Nordsletten D, Camara O, Frangi AF, Delingette H, Sermesant M, Relan J, Ayache N, Krueger MW, Schulze WHW, Hose R, Valverde I, Beerbaum P, Staicu C, Siebes M, Spaan J, Hunter P, Weese J, Lehmann H, Chapelle D, Razavi R. euHeart: personalized and integrated cardiac care using patient-specific cardiovascular modelling. *Interface Focus* 2011. DOI: 10.1098/rsfs.2010.0048.
5. Huyghe JM, Arts T, Van Campen DH, Reneman RS. Porous medium finite element model of the beating left ventricle. *American Journal of Physiology - Heart and Circulatory Physiology* 1992; **262**:1256–1267.

6. Chapelle D, Gerbeau J-F, Sainte-Marie J, Vignon-Clementel I. A poroelastic model valid in large strains with applications to perfusion in cardiac modeling. *Computational Mechanics* 2010; **46**:91–101. DOI: 10.1007/s00466-009-0452-x.
7. Rohan E, Cimrman R, Lukeš V. Numerical modelling and homogenized constitutive law of large deforming fluid saturated heterogeneous solids. *Computers and Structures* 2006; **84**:1095–1114.
8. Coussy O. *Poromechanics*. Wiley: Chichester, 2004.
9. Kassab GS, Rider CA, Tang NJ, Fung YC. Morphometry of pig coronary arterial trees. *American Journal of Physiology - Heart and Circulatory Physiology* 1993; **265**(1):H350–H365.
10. Spaan JAE, ter Wee R, van Teeffelen JWGE, Streekstra G, Siebes M, Kolyva C, Vink H, Fokkema DS, VanBavel E. Visualisation of intramural coronary vasculature by an imaging cryomicrotome suggests compartmentalisation of myocardial perfusion areas. *Medical and Biological Engineering and Computing* 2005; **43**(4):431–435.
11. Cookson AN, Lee J, Michler C, Chabiniok R, Hyde E, Nordsletten DA, Sinclair M, Siebes M, Smith NP. A novel porous mechanical framework for modelling the interaction between coronary perfusion and myocardial mechanics. *Journal of Biomechanics* 2011; **1992**:1–6.
12. Cimrman R, Rohan E. On modelling the parallel diffusion flow in deforming porous media. *Mathematics and Computers in Simulation* 2007; **76**(1-3):34–43.
13. Loula AFD, Rochinha FA, Murad MA. Higher-order gradient post-processings for second-order elliptic problems. *Computer Methods in Applied Mechanics and Engineering* 1995; **128**(34):361–381.
14. Vankan WJ, Huyghe JM, Drost MR, Janssen JD, Huson A. A finite element mixture model for hierarchical porous media. *International Journal of Numerical Methods in Engineering* 1997; **40**:193–210.
15. Malta SMC, Loula AFD, Garcia ELM. Numerical analysis of a stabilized finite element method for tracer injection simulations. *Computer Methods in Applied Mechanics and Engineering* 2000; **187**(12):119–136.
16. Babuška I. Error bounds for finite element methods. *Numerische Mathematik* 1971; **16**:322–333.
17. Brezzi F. On the existence, uniqueness and approximation of saddle point problems arising from Lagrangian multipliers. *Revue française d'automatique, informatique, recherche opérationnelle (R.A.I.R.O.). Analyse numérique* 1974; **8**:129–151.
18. Masud A, Hughes TJR. A stabilized mixed finite element method for Darcy flow. *Computer Methods in Applied Mechanics and Engineering* 2002; **191**:4341–4370.
19. Hughes TJR, Masud A, Wan J. A stabilized mixed discontinuous Galerkin method for Darcy flow. *Computer Methods in Applied Mechanics and Engineering* 2006; **195**:3347–3381.
20. MUMPS: a multifrontal massively parallel sparse direct Solver. Available from: http://graal.ens-lyon.fr/mumps/.
21. van Horssen P, Siebes M, Hoefer I, Spaan JAE, van den Wijngaard JPHM. Improved detection of fluorescently labeled microspheres and vessel architecture with an imaging cryomicrotome. *Medical and Biological Engineering and Computing* 2010; **48**(8):735–744.
22. Lamata P, Niederer S, Nordsletten D, Barber DC, Roy I, Hose DR, Smith N. An accurate, fast and robust method to generate patient-specific cubic Hermite meshes. *Medical Image Analysis* 2011; **15**:801–813.
23. Goyal A, Lee J, Lamata P, van den Wijngaard J, van Horssen P, Spaan J, Siebes M, Grau V, Smith N. Model-based vasculature extraction from optical fluorescence cryomicrotome images. *IEEE Transactions on Medical Imaging*.
24. Lee J, Niederer S, Nordsletten D, Le Grice I, Smail B, Kay D, Smith N. Coupling contraction, excitation, ventricular and coronary blood flow across scale and physics in the heart. *Philosophical Transactions of the Royal Society A: Mathematical, Physical and Engineering Sciences* 2009; **367**(1896):2311–2331.